Journal of Applied Fluid Mechanics, Vol. 18, No. 11, pp. 2791-2809, 2025.
Available online at www.jafmonline.net, ISSN 1735-3572, EISSN 1735-3645.
https://doi.org/10.47176/jafm.18.11.3453

Effect of Novel Stepped Airfoil Fin Inserts on Heat Transfer Enhancement and Fluid Flow Characteristics of Printed Circuit Heat Exchanger

A. P. Raji[1†], S. Ranganathan[2], B. S. Arputharaj[3] and V. Raja[1]

[1] *Department of Aeronautical Engineering, Kumaraguru College of Technology, Coimbatore 641049, Tamil Nadu, India*
[2] *Department of Mechanical Engineering, SNS College of Technology, Coimbatore-641107, Tamil Nadu, India*
[3] *Department of Research and Innovation, Saveetha School of Engineering, SIMATS, Chennai-602105, Tamil Nadu, India*

†*Corresponding Author Email: arulprakash.aeu@kct.ac.in*

ABSTRACT

In recent years, researchers have shown considerable interest in supercritical carbon dioxide (sCO_2) Brayton cycle-based power plants due to their unique characteristics and higher efficiency compared with conventional Rankine cycle systems. The printed circuit heat exchanger (PCHE) is a key component that significantly influences the performance of the sCO_2 cycle, owing to its compact structure and high surface area-to-volume ratio. However, designing efficient and compact PCHEs continues to be a significant challenge, mainly because it requires balancing heat transfer effectiveness with pressure drop, a task made more complex by the intricate configuration of micro-channels. This study aims to investigate the impact of airfoil fin geometry modifications on heat transfer enhancement in PCHEs using the ANSYS Fluent computational tool. Ten novel stepped airfoil fin models were introduced and analysed. The results demonstrate that airfoil fin model 9, characterised by a double-stepped profile and a flattened trailing edge, achieves a 28% increase in heat transfer rate and a 27.37% improvement in the Nusselt number compared with the baseline airfoil fin design under various operating conditions. These improvements are attributed to enhanced turbulence generated by the stepped profile, which promotes more effective convective heat transfer.

Article History

Received February 20, 2025
Revised June 3, 2025
Accepted June 29, 2025
Available online September 3, 2025

Keywords:

Printed circuit heat exchanger
Recuperator
Stepped airfoil fin
Thermohydraulic
sCO_2 power cycle

1. INTRODUCTION

1.1. Supercritical CO_2 Brayton cycle

The supercritical carbon dioxide (sCO_2) Brayton cycle is an advanced power generation system that utilises CO_2 in its supercritical state as the working fluid. This cycle has attracted attention as a promising alternative to conventional power cycles, such as the steam Rankine cycle and gas turbines, owing to its superior efficiency and distinct thermophysical properties (In & Hee, 2013; Dong et al., 2021). The printed circuit heat exchanger (PCHE) is a highly compact and efficient solution for supercritical CO_2 power conversion systems. Among the available channel configurations, the airfoil fin structure has been investigated for its excellent thermal-hydraulic characteristics (Ganeshkumar et al., 2024). Nevertheless, a direct experimental comparison between the optimised airfoil fin and the widely adopted wavy channel design remains lacking (Yu-Ming et al., 2021; Joo Hyun & Moo Hwan, 2024). Incorporating a CO_2/H_2S mixture significantly improves heat transfer in airfoil fin channels, while small quantities of H_2S have a negligible effect on frictional resistance. Additionally, buoyancy contributes positively to heat transfer enhancement in these configurations (Haiyan et al., 2024; Sheikholeslami et al., 2024a, b, c). The best thermal-hydraulic performance was achieved under transcritical conditions, surpassing both near- and far-critical states. The newly optimised airfoil fin design matched the overall performance of traditional airfoil fins while reducing fin volume by 50%, enabling a lighter PCHE design. However, performance deteriorated when the fin height was slightly less than the channel height, highlighting a critical design consideration (Kumar et al., 2023; Raghunath et al., 2023; Kun, et al., 2023).

Recent advances in integrating sCO_2 into gas turbine engines have provided notable benefits across various power plant applications, including improved engine efficiency

NOMENCLATURE

Nu	Nusselt number	W	width of the channel
f	fanning friction factor	h	heat transfer coefficient
L_v	vertical pitch length	Pr	Prandtl number
L_s	staggered pitch length	j	Colburn factor
k-ε	turbulent kinetic energy-dissipation rate	L_a	airfoil chord Length
I_t	turbulent intensity	ρ	density
L	length of the channel	W_a	maximum thickness of airfoil

and reduced system size (Lei et al., 2014a; Su-Jong et al., 2014). The selection of sCO_2 for the Brayton cycle is driven by its advantageous characteristics, which combine the properties of both liquids and gases, especially in its supercritical phase (Sandeep et al., 2014; Tae et al., 2015). When CO_2 is heated and compressed beyond its critical point (7.38 MPa, 31°C), it exhibits a unique combination of low viscosity, low compressibility, and high density, making it an ideal working fluid for sustaining the Brayton cycle efficiently (Ishizuka et al., 2006; Seo et al., 2015; Xu et al., 2015).

Additionally, sCO_2 serves as an efficient medium for both heat transfer and work execution within the cycle, owing to its non-toxic and chemically stable properties (Seong et al., 2016; Kodi et al., 2022). Compared with helium, sCO_2 offers easier compression due to its high density, which is comparable to that of a liquid (Ajinkya et al., 2016; Yu-Ming et al., 2021). While operating temperatures remain moderate, cycle efficiency can be improved by optimising compressor design and minimising the size of heat exchangers and turbines (Jin et al., 2016; Minghui et al., 2016).

A comprehensive study was conducted to evaluate the thermohydraulic performance and pressure drop characteristics of the PCHE model. This analysis combined computational and experimental methodologies, employing ANSYS Fluent software to simulate sCO_2 flow behaviour. Experimental findings by Xu et al. revealed that the airfoil fin PCHE experienced significantly lower pressure loss than the zigzag channel. Moreover, the airfoil fin PCHE demonstrated a higher heat transfer rate per unit volume compared with the zigzag channel (Baik et al., 2016; Kodi et al., 2022; Usman et al., 2022; Yun-Jie et al., 2022).

This study aims to bridge the existing knowledge gap by numerically analysing the thermal-hydraulic performance of novel stepped airfoil fin inserts in PCHE channels. Using validated computational fluid dynamics (CFD) simulations, the work evaluates heat transfer enhancement and pressure drop characteristics across different Reynolds number regimes and compares the results with conventional fin configurations. The findings contribute to the design optimisation of PCHEs for advanced energy applications.

The present research primarily focuses on improving heat transfer performance using innovative airfoil-shaped fins. These fins are uniquely designed based on inspiration drawn from the Küchemann–Flettner–Munk (KFM) series airfoils, known for their aerodynamic efficiency. By leveraging the geometric and flow characteristics of KFM airfoils, the study aims to optimise fin configurations that enhance thermal performance, reduce flow resistance, and increase the overall effectiveness of heat exchangers.

1.2. Related Literature

Dong et al. (2021) conducted an experiment to assess the thermohydraulic characteristics of PCHE. The results indicated a slight increase in the heat transfer rate as the system approached critical pressure, primarily attributed to rising values of the Prandtl number. Additionally, a distinct relationship was established between the friction factor, pressure drop, and Reynolds number, with all these parameters increasing proportionally to the Reynolds number.

Saeed et al. (2017) conducted a study to evaluate the thermohydraulic performance of a PCHE by examining different fluid combinations, including water, helium–carbon dioxide, and helium–water. The researchers employed both CFD simulations and experimental data to derive their conclusions. Their findings revealed a significant increase in the heat transfer rate as the system neared critical pressure, primarily due to the rising Prandtl number.

Su-Jong et al. (2014) performed a computational analysis on crossflow PCHEs used in advanced compact modular reactors. The study aimed to evaluate the impact of various operating conditions on the characteristics of sCO_2 fluid. Additionally, a comprehensive cost analysis of the heat exchanger was conducted by comparing the calculated temperature distribution with the specific temperature requirements of each SMR. The sensitivity test results demonstrated that the grid had minimal influence on the temperature distribution. The study also found that the computational model used was as effective as the widely adopted e-NTU method. The results highlighted a strong correlation between temperature and heat transfer, which significantly affects the local temperature distribution. Furthermore, the findings revealed that helium gases exhibited notable variations in the crossflow PCHE due to heat transfer effects. Conversely, as the Prandtl number increased, the relationship between heat transfer and temperature weakened, resulting in a reduced difference between these two variables.

Xu et al. (2015) conducted a study on PCHEs to assess their heat transfer efficiency and flow resistance. The researchers performed experimental tests using two different configurations. One setup featured a staggered arrangement, while the other used a parallel pattern. The purpose of these tests was to determine which configuration provided the most effective performance for the airfoil fin design. Additionally, numerical analyses were performed to evaluate the impact of varying input

velocities, with values of 0.5, 1.0, 2.5, 4.0, and 5.0 m/s corresponding to Reynolds numbers of 12,517, 25,035, 62,588, and 100,140, respectively. The findings revealed that the staggered fin configuration significantly improved heat transfer efficiency while reducing flow resistance. Furthermore, an advanced airfoil fin design was implemented to minimise pressure loss and enhance heat transfer performance.

Lei et al. (2014b) conducted a study using a CFD model to analyse the impact of various factors on the pressure drop and heat transfer efficiency of an airfoil-shaped PCHE. The research examined multiple variables, including the Reynolds number, fin row count, and the transverse and longitudinal pitches of the airfoil fin. The primary objective was to evaluate PCHE performance when integrated with different airfoil designs. The findings revealed a negative correlation between the friction factor, the Nusselt number, and the transverse and longitudinal fin pitches, aligning with the experimental data.

Sandeep et al. (2014) conducted an experimental study to investigate the influence of buoyancy on the thermal conductivity properties of sCO_2 during heating. The study involved exposing sCO_2 to various operating pressures, up to a maximum of 10.2 MPa, and Reynolds numbers reaching 60,000. Controlled experiments were performed on horizontal, upward, and downward flows to analyse the effects of buoyancy on heat convection. The results indicated that when the bulk temperature falls below the pseudocritical temperature, buoyancy significantly impacts all system orientations.

Seo et al. (2016) conducted a study using CFD to assess the performance of a PCHE in an sCO_2 power Brayton cycle. The aerodynamically designed fins enhanced the heat exchanger's cooling efficiency. Researchers utilised ANSYS CFX to simulate various conditions, adjusting parameters such as mass flow rates, Reynolds numbers, and fin configurations. The findings revealed that higher Reynolds numbers and mass flow rates improved heat transfer while reducing pressure losses due to acceleration. Additionally, a fully staggered fin arrangement resulted in a 40% greater pressure reduction compared with an unstaggered configuration.

Seo et al. (2015) conducted an empirical study to evaluate heat transfer and pressure reduction in straight-channel PCHEs. The research involved experimental trials using a PCHE prototype, where the high-temperature side was exposed to fluid temperatures between 40°C and 50°C, while the low-temperature side was maintained at a constant 20°C. The study examined Reynolds numbers ranging from 100 to 850. A comparative analysis of parallel and counterflow designs demonstrated a significant improvement in heat transfer efficiency, ranging from 6.8% to 15%. Higher Reynolds numbers led to an increased average heat transfer rate and a reduced pressure gradient. Additionally, the data indicated that increasing the inlet temperature caused a slight decrease in pressure drop.

Xinying et al. (2018) demonstrated that PCHEs play a crucial role in ensuring the efficient operation of the sCO_2 Brayton cycle. Previous studies have established a strong empirical correlation between the pressure drop factor and the heat transfer coefficient, which remains consistent across a wide range of Reynolds numbers. The Reynolds number serves as a key parameter for quantifying fluid resistance during the flow process. Xu et al. (2015) conducted a numerical study on PCHEs to evaluate the thermal-hydraulic performance of various non-continuous fin designs. The primary objective was to analyse the impact of different fin configurations on the thermohydraulic efficiency of the PCHE. Computational results revealed that at low sCO_2 mass flow rates, fin design has minimal effect on thermal-hydraulic performance. The study found that altering fin positioning does not significantly impact efficiency. Among the designs tested, the airfoil fin PCHE exhibited superior thermohydraulic performance, surpassing previous fin configurations, while the rounded rectangular fin (RRF) was found to be less efficient than other commonly used designs.

Baik et al. (2016) conducted a study to assess the thermohydraulic performance of a PCHE by analysing various fluid combinations, including water, helium–carbon dioxide, and helium–water. To achieve this, the researchers utilised both CFD simulations and experimental data. The results indicated a notable enhancement in heat transfer rates as the critical pressure was approached, attributed to the increase in the Prandtl number. Ajinkya et al. (2016) conducted a comprehensive analysis of PCHEs within the context of an sCO_2 power cycle. Their findings underscored the efficiency of PCHEs, regardless of the delivery method. Research on sCO_2 Brayton cycles has demonstrated that variations in hydraulic diameter and Reynolds number have a significant impact on heat transfer rates and pressure drops. The results showed that zigzag channels outperform straight channels, especially when the zigzag bend angles are larger and the linear pitch is smaller. When comparing heat transfer performance, zigzag channels exhibit greater efficiency than straight channels of the same length. Jin et al. (2016) conducted a study to enhance the efficiency of a small-scale Brayton cycle by integrating an airfoil-type PCHE. To assess its performance, experiments were performed using various airfoil designs and operating conditions to analyse heat transfer and pressure drop behaviour. The study aimed to optimise the design for cost reduction. The findings established new correlations between heat transfer and pressure drop in PCHEs featuring airfoil fins. Wen-xiao et al. (2016) examined the heat transfer and pressure drop characteristics of a PCHE operating at high temperatures. The heat exchanger featured both circular and straight channels, with helium used as the working fluid. The results indicated that zigzag channels provide superior heat transfer performance compared with circular, straight channels. However, due to the increased curvature in zigzag channels, the pressure drops more rapidly than in the straight, circular configuration.

The study by Baik et al. (2016) conducted a thorough investigation into the operational efficiency of sCO_2–water PCHEs across different CO_2 concentrations. The research combined mathematical modelling with

experimental analysis. In sCO_2 systems, the precooler typically operates near CO_2's critical point, but traditional design methods may fall short due to changes in thermophysical properties at this critical point. The main goal of the study was to validate the accuracy of PCHE core design codes and assess the experimental test results. The experiments involved temperature variations between 26 and 43°C, and pressure changes ranging from 7.3 to 8.6 MPa. The Reynolds number varied between 15,000 and 100,000, while the Prandtl number was limited to a range of 2 to 23. By combining experimental data with computational modelling, the researchers determined the friction factor and established correlations between heat transfer rates.

Aneesh et al. (2017) conducted a computational analysis to assess the thermohydraulic performance of PCHEs with zigzag, wave, and serpentine channel configurations. The primary goal of the study was to investigate how the thermophysical properties of sCO_2 impact the performance of different channel designs. Using modelling and numerical analysis, the researchers evaluated the performance of a single-channel PCHE core across three channel configurations under various operating conditions. The results showed that the swept-zigzag model achieved superior heat transfer efficiency compared with other designs, such as straight, zigzag, and sinusoidal wavy channels, while also producing the greatest reduction in pressure. Zhao et al. (2017) utilised CFD to examine the flow and heat transfer characteristics of supercooled sLNG. The study concentrated on a PCHE with airfoil fins to enhance performance. The airfoil fin design played a key role in improving heat transfer and reducing pressure drop for sLNG gas. Simulations indicated that staggered fin arrangements offered better thermohydraulic performance than parallel configurations. Additionally, experimental results revealed that changing from a staggered pitch (Ls) to a vertical pitch (Lv) reduced the thermohydraulic efficiency of the airfoil fin PCHE.

Fei et al. (2017) conducted an experimental study using a PCHE with straight channels to evaluate the heat transfer characteristics between sCO_2 and water. The results showed that the heat transfer rate for sCO_2 is approximately 1.2–1.5 times higher than that of water, primarily due to its higher mass flow rate. This difference in heat transfer rates is attributed to the variation in flow rates between sCO_2 and water. Further investigations examined the performance of a PCHE with linear ribs at different sCO_2 pressures, revealing that transcritical operation reduces PCHE efficiency by about 17.6% compared with standard conditions. Minghui et al. (2016) performed a CFD study on a PCHE to assess its thermohydraulic performance with airfoil fins. The results demonstrated a consistent pressure drop along the primary flow path, which remained stable, even though the heat transfer rate was reduced due to the distinct properties of sCO_2. Wen-xiao et al. (2017) carried out an extensive study to assess the efficiency of airfoils with zigzag channels in PCHEs. Their findings highlighted the relationship between airfoil thickness and heat exchanger performance, particularly in terms of heat transfer and pressure drop. The NACA0010 airfoil fin outperformed other airfoil designs with zigzag channels in terms of performance. Saeed & Kim (2017) aimed to assess the thermal-hydraulic performance of PCHEs by examining various fin shapes. The study tested a range of Reynolds numbers and geometric configurations. The results revealed an inverse relationship between fin angle and performance evaluation criteria (PEC), showing that PEC decreases as the fin angle increases. This observation applies to both low-temperature and high-temperature pipes.

Lei et al. (2017) conducted an in-depth investigation into the convective heat transfer characteristics of sCO_2, with a particular focus on the impact of low mass flow rates. The study used both experimental and numerical analyses to enhance thermohydraulic performance. The experimental results showed a substantial improvement in performance metrics when the fin angle was adjusted from 0° to 130°, resulting in a 37% increase. Zhongchao et al. (2020) conducted a study using both computational models and practical methods to analyse the operation of a PCHE with sLNG. The temperature ranged from 113 to 129°C, and the inlet pressure varied between 4.5 and 6 MPa, with the mass flow rate of sN_2 held constant at 299.94 kg/hr. Both experimental and computational results showed that increasing the input pressure improves heat transfer performance. As the inlet pressure increases, the pressure drop on the cold side of the device decreases proportionally. Sandeep et al. (2018) conducted a study using sCO_2 as the working fluid to evaluate the thermohydraulic performance of different non-continuous fin heat exchanger configurations. The tests simulated real-world conditions relevant to sCO_2 Brayton cycles. The results revealed that PCHEs with non-continuous rectangular and airfoil fin plates experienced much lower pressure loss compared with those using continuous zigzag channels. Pinaa et al. (2019) performed a computational analysis of a PCHE using supercritical carbon dioxide. The findings revealed that as the temperature rises, pressure gradients in sCO_2 become more pronounced. Furthermore, an increase in mass transfer velocity was consistently associated with a rise in heat transfer velocity, resulting in a reduction in pressure.

1.3. Author Observation and Problem Definition

The heat exchanger used in supercritical CO_2 applications accounts for a significant portion of the overall cycle cost, potentially as much as 60%. Additionally, it plays a crucial role by providing approximately 40% of the total heat needed to achieve the desired cycle performance. By using PCHEs, thermal performance can be enhanced, and pressure drop minimised through careful selection and proper manufacturing of components. A review of the literature shows that most previous studies have focused on the thermal-hydraulic performance of straight and zigzag channels, with only a limited number of investigations into airfoil fin PCHEs. There remains considerable potential for further research to improve heat transfer and reduce pressure loss in PCHEs.

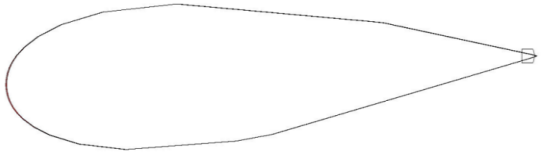

Fig. 1 Base airfoil model

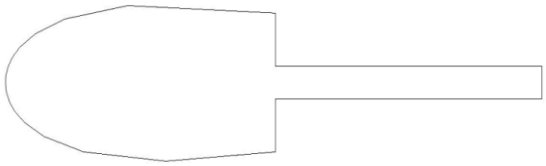

Fig. 2 Stepped airfoil model 1

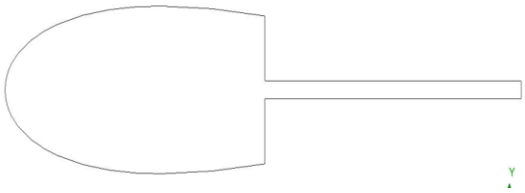

Fig. 3 Stepped airfoil model 2

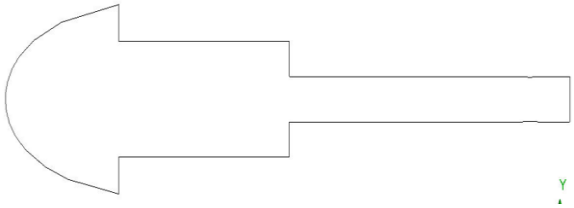

Fig. 4 Stepped airfoil model 3

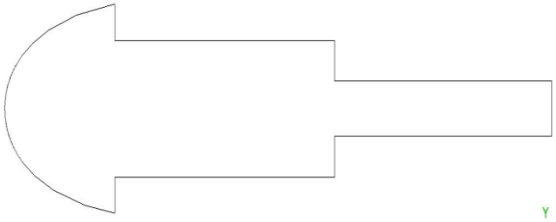

Fig. 5 Stepped airfoil model 4

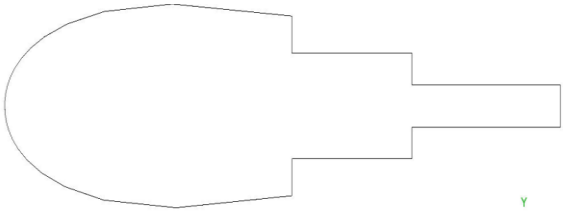

Fig. 6 Stepped airfoil model 5

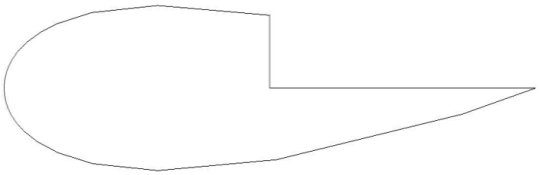

Fig. 7 Stepped airfoil model 6

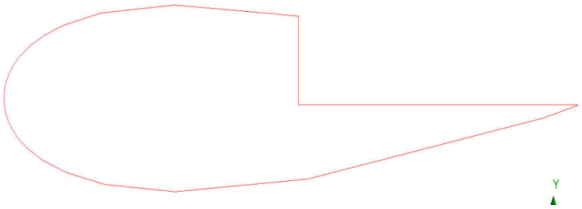

Fig. 8 Stepped airfoil model 7

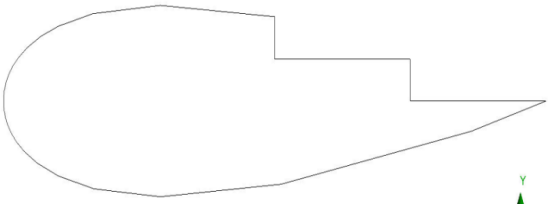

Fig. 9 Stepped airfoil model 8

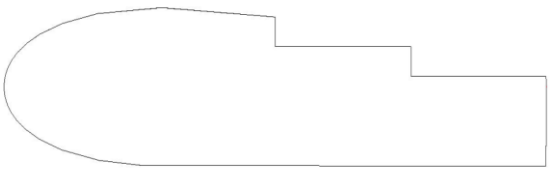

Fig. 10 Stepped airfoil model 9

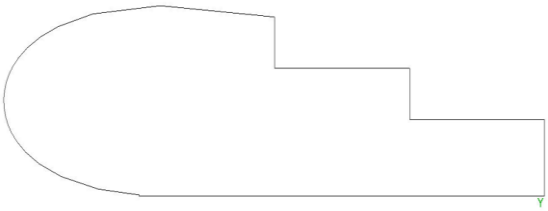

Fig. 11 Stepped airfoil model 10

The objective of the current research is to numerically analyse the heat transfer and pressure drop characteristics of an airfoil fin–printed circuit heat exchanger using sCO_2 as the working fluid. This study is conducted in three phases. Phase one begins with a grid-independent analysis to determine the optimal mesh size for the numerical simulations. In phase two, the numerical base model is validated by comparing its results to existing experimental data from a literature survey. The third phase involves a comprehensive investigation of the PCHE using 10 different stepped airfoil models, as shown in Figures 1-11. to identify a novel stepped airfoil that enhances heat transfer while maintaining a reasonable pressure drop compared with the base airfoil model.

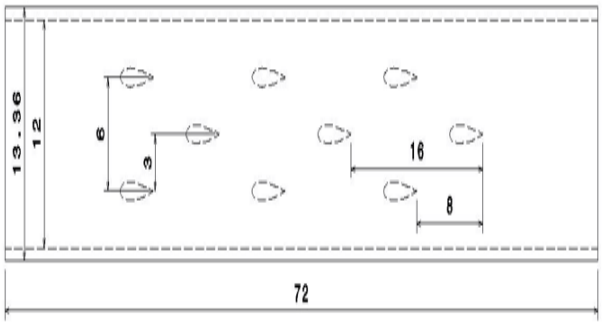

Fig. 12 Computational model of airfoil fin PCHE

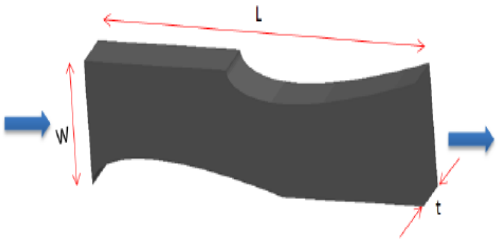

Fig. 13 Volume to define a hydraulic diameter

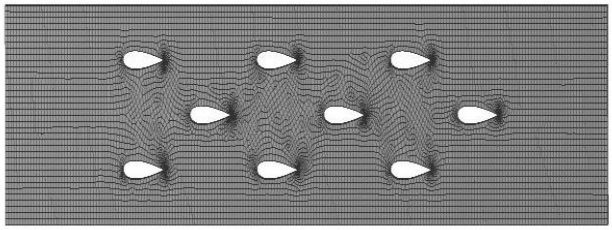

Fig. 14 Airfoil fin PCHE mesh model

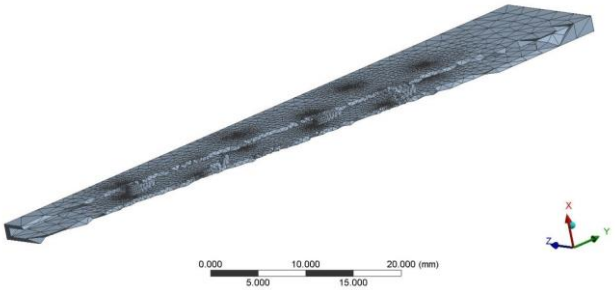

Fig. 15 3D cut section view of airfoil fin PCHE mesh model

challenging and requires high-performance computing resources. To overcome this, the study uses a single-channel airfoil fin PCHE model, enabling a simplified analysis that is compatible with the available computational capacity.

The simulation is carried out under a constant wall temperature. Figure 12 shows the geometry of the PCHE model, with a channel length (L) of 72 mm, width (W) of 12 mm, and height (H) of 1 mm. A symmetrical airfoil is chosen for this study, as cambered airfoils tend to cause more turbulence and higher pressure drops (Raji et al., 2024). The channel contains a staggered array of nine symmetrical NACA0021 airfoils, each with a chord length (L_a) of 4 mm, height (H_a) of 1 mm, and maximum thickness (W_a) of 0.96 mm. Additionally, the airfoil features a longitudinal pitch (P_l) of 8 mm and a transverse pitch (P_t) of 3 mm (Raji et al., 2024).

The hydraulic diameter (D_h) is crucial in dimensionless analysis, acting as the representative length of the channel. For a straight channel, it is calculated as four times the cross-sectional area divided by the perimeter. However, in this case, the continuous variations in cross-sectional area and perimeter lead to a hydraulic diameter that differs from that of a straight channel, as illustrated in Fig. 13. Nevertheless, the periodic arrangement of the airfoil fins, shown in Fig. 13, allows the hydraulic diameter to be defined Eqs.1- 3.

$$V = (LW - S_a)\, t \tag{1}$$

$$S = (P_a t/2) + 2(L - L_c)\, t + 2(WL - S_a) \tag{2}$$

$$D_h = 4V/S \tag{3}$$

where V, S, Sa, and Pa represent the volume, side surface area, top surface area, and perimeter of the airfoil fin, respectively.

2.1. Discretisation

Figures 14 and 15 illustrate the hybrid mesh configuration of an airfoil fin PCHE, offering both a comprehensive overall view and a cross-sectional perspective, respectively. Advanced meshing techniques have been utilised in this study to improve the accuracy of the numerical results. To achieve more precise results, particularly on the surface wall of the airfoil fin, a tetrahedron mesh is used, as shown in Fig. 14.

2.2. Governing Equations

The commercial software ANSYS FLUENT is used for the calculations in this study, with the governing equations listed below. These equations are implemented in the CFD code to compute the values of pressure, density, temperature, and velocity components. The governing equations used in CFD are presented in Eqs. (4) to (11). The continuity equation ensures the conservation of mass in all non-nuclear continuum mechanics analyses. It is derived by integrating the rates at which mass enters and exits the control volume, equating the inflow rate to the rate of mass accumulation within the volume. The principle of mass conservation states that mass is neither created nor destroyed in a closed system. Equation (4) represents the continuity equation (Raji et al., 2024):

$$\frac{D\rho}{Dt} + \left[\rho * \left(\frac{\partial u}{\partial x} + \frac{\partial v}{\partial y} + \frac{\partial w}{\partial z}\right)\right] = 0 \tag{4}$$

The variables in question are ρ, denoting density, and u, v, w, representing the velocity vector in the x, y, and z directions. The momentum equation is essentially derived from Newton's second law of motion, which states that force is equal to the product of mass and acceleration. The momentum equations are denoted by Eqs. (5), (6), and (7) (Wen-xiao et al., 2017):

$$\rho_F g_{x,F} - \frac{\partial P_F}{\partial x} + \frac{\partial}{\partial x}\left(\mu_F\left(2 * \frac{\partial u_F}{\partial x} - \frac{2}{3} * \nabla.\overrightarrow{V_F}\right)\right) + \frac{\partial}{\partial y}\left(\mu_F\left(\frac{\partial v_F}{\partial x} + \frac{\partial u_F}{\partial y}\right)\right) + \frac{\partial}{\partial z}\left(\mu_F\left(\frac{\partial w_F}{\partial x} + \frac{\partial u_F}{\partial z}\right)\right) = \rho_F\left(\frac{\partial u_F}{\partial t} + u_F\frac{\partial u_F}{\partial x} + v_F\frac{\partial u_F}{\partial y} + w_F\frac{\partial u_F}{\partial z}\right) \quad (5)$$

$$\rho_F g_{y,F} - \frac{\partial P_F}{\partial y} + \frac{\partial}{\partial x}\left(\mu_F\left(\frac{\partial v_F}{\partial x} + \frac{\partial u_F}{\partial y}\right)\right) + \frac{\partial}{\partial y}\left(\mu_F\left(2 * \frac{\partial v_F}{\partial y} - \frac{2}{3} * \nabla.\overrightarrow{V_F}\right)\right) + \frac{\partial}{\partial z}\left(\mu_F\left(\frac{\partial w_F}{\partial y} + \frac{\partial v_F}{\partial z}\right)\right) = \rho_F\left(\frac{\partial v_F}{\partial t} + u_F\frac{\partial v_F}{\partial x} + v_F\frac{\partial v_F}{\partial y} + w_F\frac{\partial v_F}{\partial z}\right) \quad (6)$$

$$\rho_F g_{z,F} - \frac{\partial P_F}{\partial z} + \frac{\partial}{\partial x}\left(\mu_F\left(\frac{\partial w_F}{\partial x} + \frac{\partial u_F}{\partial z}\right)\right) + \frac{\partial}{\partial y}\left(\mu_F\left(\frac{\partial v_F}{\partial z} + \frac{\partial w_F}{\partial y}\right)\right) + \frac{\partial}{\partial z}\left(\mu_F\left(2 * \frac{\partial w_F}{\partial z} - \frac{2}{3} * \nabla.\overrightarrow{V_F}\right)\right) = \rho\left(\frac{\partial w_F}{\partial t} + u_F\frac{\partial w_F}{\partial x} + v_F\frac{\partial w_F}{\partial y} + w_F\frac{\partial w_F}{\partial z}\right) \quad (7)$$

The u_F, v_F, w_F represent velocity vector fluid in the x, y, and z directions, respectively. The $P_F, \rho_F, and\ \mu_F$ denote pressure, density, and viscosity of the fluid. The variable V_F is the divergent velocity vector of all the velocities. The $g_{x,F}$, $g_{y,F}$, $g_{z,F}$, represent gravitational force in the x, y, and z directions, respectively.

The energy equation is derived from the First Law of Thermodynamics, which establishes the principle of energy conservation. This law states that, in an open system, the rate of energy change within the control volume must be equal to the net outflow of energy across the control volume boundaries. The net energy outflow includes the outflow of internal energy, kinetic energy, work, and heat. The energy equation is expressed in Eq. (8) (Gopinath et al., 2024; Raji et al., 2024):

$$\rho_F\left[\left(\frac{\partial U_F}{\partial t} + \frac{\partial U_F}{\partial x} + \frac{\partial U_F}{\partial y} + \frac{\partial U_F}{\partial z}\right)\right] = \left[\frac{\partial}{\partial x}\left(k_F.\frac{\partial T_F}{\partial x}\right) + \frac{\partial}{\partial y}\left(k_F.\frac{\partial T_F}{\partial y}\right) + \frac{\partial}{\partial z}\left(k_F.\frac{\partial T_F}{\partial z}\right)\right] + \sigma_{xx,F}\frac{\partial u_F}{\partial x} + \sigma_{yy,F}\frac{\partial v_F}{\partial x} + \sigma_{zz,F}\frac{\partial w_F}{\partial x} + \left[\tau_{xy,F}\left(\frac{\partial v_F}{\partial x} + \frac{\partial u_F}{\partial y}\right)\right] + \left[\tau_{yz,F}\left(\frac{\partial w_F}{\partial y} + \frac{\partial v_F}{\partial z}\right)\right] + \left[\tau_{xz,F}\left(\frac{\partial u_F}{\partial z} + \frac{\partial w_F}{\partial x}\right)\right] \quad (8)$$

where ρ_F, U_F, T_F, and k_F represent density, internal energy, temperature, and thermal conductivity of the fluid. component velocity magnitudes in x, y, and z directions. $\tau_{xy,F}, \tau_{yz,F}, \tau_{xz,F}$ indicate viscosity stress in the xy, yz, and xz co-ordinates, respectively. The u_F, v_F, and w_F represent velocity vector fluid in the x, y, and z directions, respectively. The $\sigma_{xx,F}, \sigma_{yy,F}, \sigma_{zz,F}$ represent primary shear force acting along the xx, yy, and zz directions, respectively. The Navier-Stokes equation is used to describe the flow of frictionless and incompressible fluids. It also encompasses the principles of mass and momentum conservation for Newtonian fluids. The equation is expressed in Eq. (9) [28]:

$$\rho.\left(\frac{\partial v}{\partial t} + (v.\nabla)v\right) = \nabla p + \rho g + \mu\nabla^2 v \quad (9)$$

The equation $\nabla p + \rho g + \mu\nabla^2 v$ represents the total forces acting on the fluid, including pressure gradient, gravitational forces, and internal stress. In this equation, v denotes the velocity of an incompressible fluid, ρ signifies the mass density, and $(\partial v/\partial t + (v\cdot\nabla)v)$ represents the acceleration. The k-epsilon (k-ε) turbulence model is commonly employed to simulate turbulent flow conditions. This model specifically targets the parameters that affect turbulent kinetic energy. The standard k-ε model is chosen when the number of unknowns is minimal. It consists of two equations involving the turbulent kinetic energy (k) and the turbulent dissipation rate (ε). The turbulence equations are expressed as Eqs. (10) and (11) (Thangaraj et al., 2023; Raji et al., 2024; Gopinath et al., 2024):

$$k_e = \frac{3}{2}(VI_t)^2 \quad (10)$$

where, k_e is the turbulent kinetic energy; I_t is the turbulent intensity; V is the mean flow velocity (Raji et al., 2024).

$$\varepsilon_r = C_\mu^{\frac{3}{4}}\frac{(k_e)^{\frac{3}{2}}}{l} \quad (11)$$

where, ε_r is the turbulence dissipation rate; C_μ is the constant of turbulence model; k_e is the turbulence energy; l is the turbulent length scale (Raji et al., 2024).

There are many dimensionless numbers that represent heat transfer and pressure drop characteristics. However,

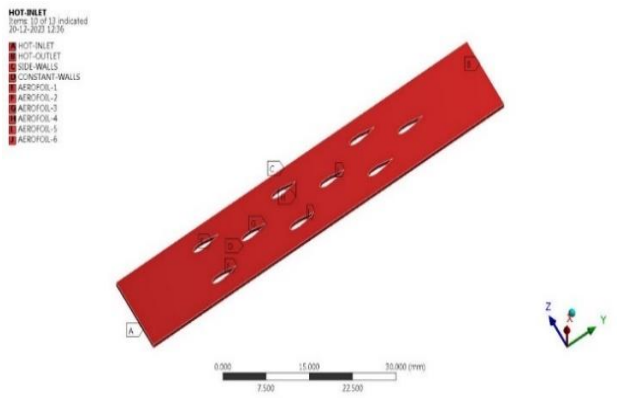

Fig. 16 Boundary names of the PCHE computational domain

the Colburn j-factor and Darcy friction factor (f) are widely used to express the heat transfer performance of a heat exchanger.

$$\text{Colburn factor (j)} = Nu/ (Re.\ Pr^{1/3}) \quad (12)$$

where Nu is Nusselt number, Pr is Prandtl number, and Re is Reynolds number.

$$Nu = (hD_h /k) \quad (13)$$

$$Re = (\rho.v.D_h)/ \mu \quad (14)$$

$$Pr = \mu C_p/k \quad (15)$$

where μ, C_p, and v represent the dynamic viscosity, specific heat capacity, and velocity respectively, and h is the heat transfer coefficient, and k is the thermal conductivity of the working fluid.

$$\text{Darcy friction factor (f)} = (\Delta P.\ D_h)/ (2v^2.\rho.L) \quad (16)$$

where ΔP and D_h represent the pressure drop and the hydraulic diameter of the channel, respectively.

2.3. Boundary Conditions

Figure 16 shows the boundary names applied to the computational domain of the PCHE. The model includes a velocity inlet and a pressure outlet. The inlet boundary conditions specify a velocity of 0.5 m/s and a temperature of 550 K, while a pressure of 8 MPa is set at the outlet. Both the top and bottom walls are maintained at a constant wall temperature of 330 K, and the side walls are treated as adiabatic. The key assumptions include steady-state, single-phase flow of real-gas sCO_2 with temperature-dependent properties. The flow is considered incompressible at low Mach numbers, with no-slip walls and negligible radiation. Boundary conditions typically involve constant wall temperature, and periodic boundaries are used to reduce computational cost. Wall and fin surfaces are assumed smooth, and mesh independence and solution convergence are ensured for accuracy. To accurately capture the fluid's thermal properties in the fluid–structure interaction region, a k-ε enhanced wall treatment turbulence model is applied (Chhaparwal, et al. 2024; Karthigairajan et al. 2025, Veeraperumal Senthil Nathan et al. 2025). The solid

Table 1 Thermo physical properties of sCO_2

S. No	Properties	Value
1	Specific heat capacity (Cp) (kJ/kgK)	1133
2	Density (kg/m^3)	80.49
3	Thermal Conductivity (K)	0.039
4	Dynamic Viscosity Ns/m^2	2.658 e10^{-5}

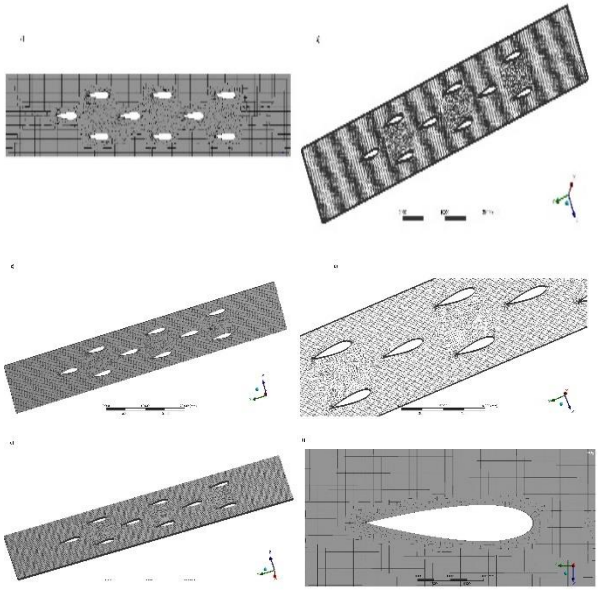

Fig. 17 Hybrid mesh over airfoil fin PCHE a) Case 1, b) Case 2, c) Case 3, 4) Case 4, 5) Case 5, 6) Case 6

domain is modelled with the material properties of stainless steel SS316L. Since the density-based solver is unsuitable for this study, which involves low-speed flow, a pressure-based solver is used to achieve accurate solutions. The thermophysical properties of supercritical CO_2 are obtained from the NIST REFPROP database and incorporated into the Fluent library. The thermophysical properties of the working fluid are shown in Table 1 (Gopinath et al., 2024; Raji et al., 2024).

2.4. Grid Refinement Study

A grid refinement study was conducted on the airfoil fin PCHE to validate and ensure the accuracy of the selected mesh model. This study was conducted for six different element sizes, including the base model, resulting in a range of elements from 635,992 to 4,886,097. Figs 17a) to f) illustrate the hybrid mesh model of the base PCHE for Cases 1 through 6.

Figures 18a) to f) display the temperature distribution along the channel, revealing a significant drop in outlet temperature from Cases 1 to 4, while in Cases 5 and 6, the outlet temperature remains unchanged despite variations in element size (Raji et al., 2024).

Figure 19 illustrates the variation in outlet temperature for all six hybrid mesh cases. The results indicate that the channel outlet temperature rises for the initial cases, but as the number of elements increases in Cases 4 and 5, the values become saturated. The temperature reaches saturation at an average of 395.23 K (Raji et al., 2024).

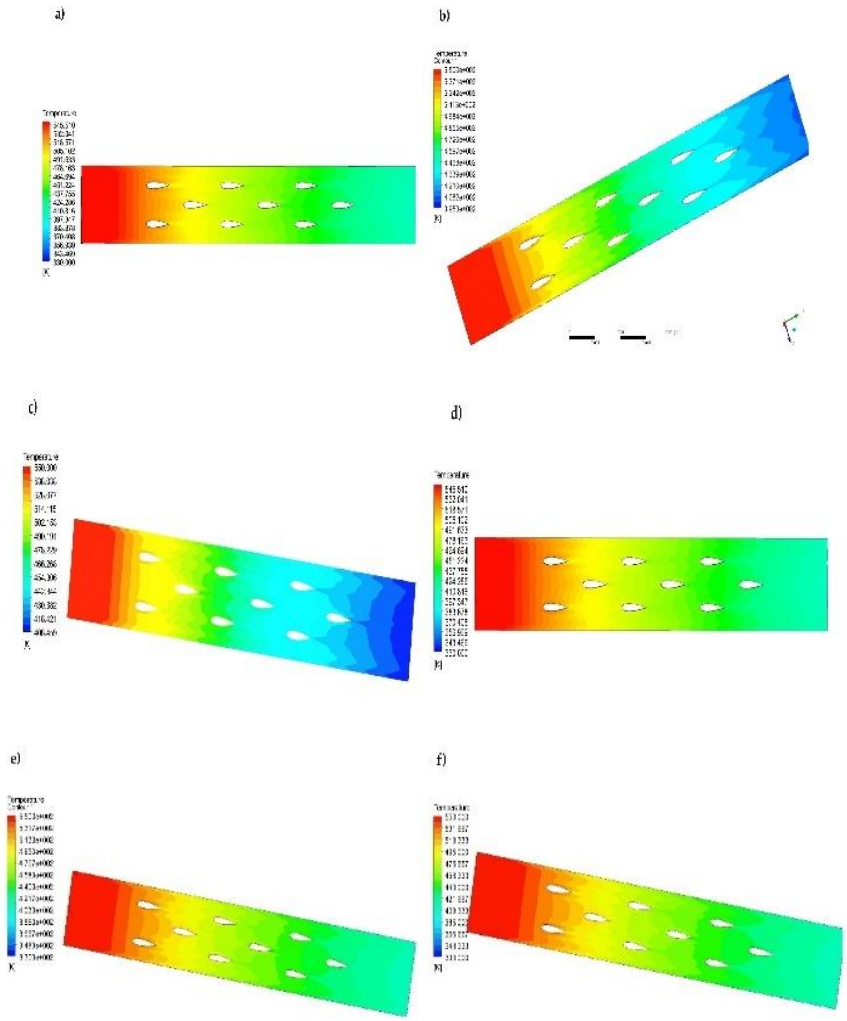

Fig. 18 Temperature distribution over an airfoil fin PCHE a) Case 1, b) Case 2, c) Case 3, 4) Case 4, 5) Case 5, 6) Case 6

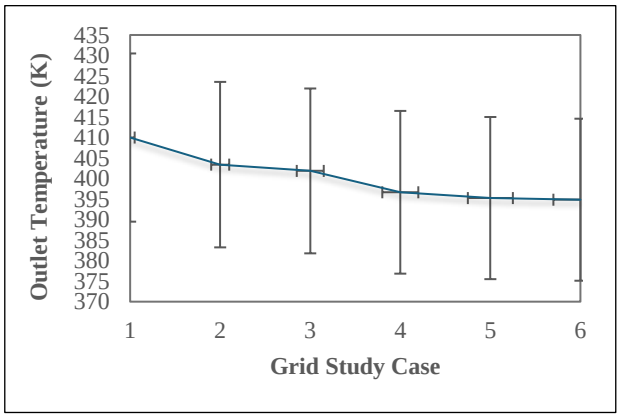

Fig. 19 Grid refinement study result comparison

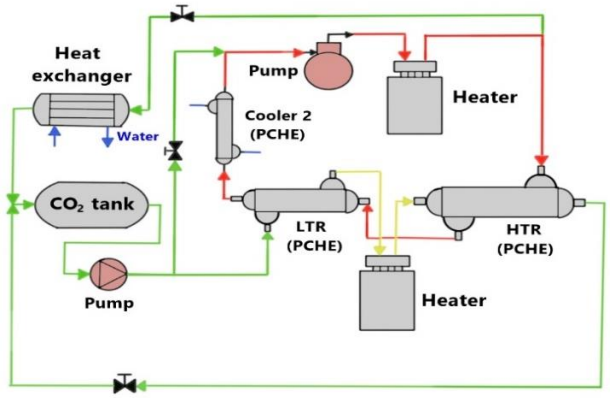

Fig. 20 Typical layout of experimental test setup

2.5. Experimental Correlation Test

In the study by Haiyan et al. (2021), experimental conditions were applied to verify and validate the accuracy of the numerical results. The same experimental operating conditions were used as boundary conditions for this numerical analysis to validate the model. Figure 20 shows the typical setup of an experimental test rig for the PCHE using sCO_2 as the working fluid. The system includes a low-temperature recuperator, a high-temperature recuperator, a cooler, and a heater, arranged sequentially.

The outlet pressure is 8.43 MPa, the mass flow rate is 0.15 kg/s, and the inlet temperature is set to 358.7 K for a PCHE channel. The top and bottom surfaces of the computational domain are kept at a constant wall temperature of 289.5 K,

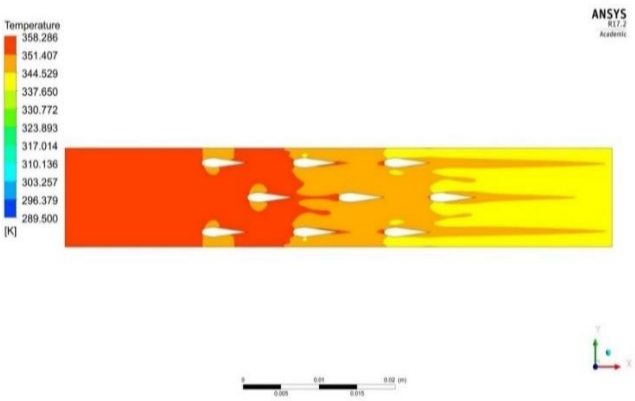

Fig. 21 Temperature distribution on airfoil fin PCHE

Table 2 Comparisons of experimental and numerical results

Parameter	Experimental data	Numerical results	Error Percentage (%)
Temperature outlet in (K)	291.5	306.3	4.83
Pressure drop (Δp) in (kPa)	90	87	3.33

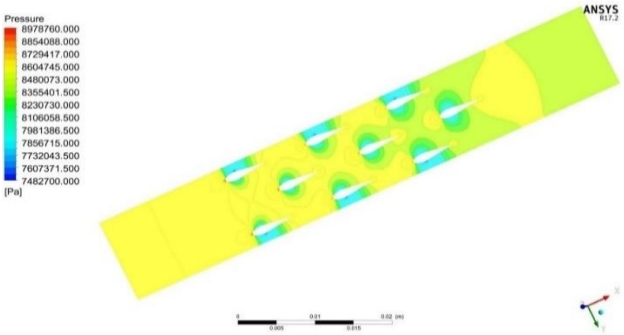

Fig. 22 Pressure variation over airfoil fin PCHE

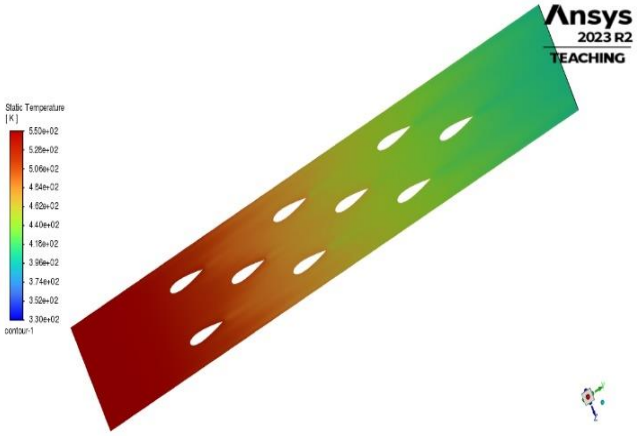

Fig. 23 Temperature distribution over an airfoil fin PCHE

while the side walls are treated as adiabatic. A hybrid mesh was used in the computational model (Raji et al., 2024).

The simulation was performed under the specified boundary conditions using ANSYS Fluent, and the resulting numerical outcomes are shown in Figs 21 and 22. Figure 21 illustrates the temperature distribution across a single channel of the airfoil fin PCHE. The results indicate that the outlet temperature decreased from the inlet temperature of 358.7 K to 306.3 K (Raji et al., 2024).

Figure 22 illustrates the pressure variation across the airfoil fin PCHE channel. The results indicate a significant pressure drop from the inlet to the outlet, which is caused by the local acceleration of the fluid over the airfoil surface (Raji et al., 2024).

The results presented in Table 2 show good agreement between experimental and numerical investigations of the airfoil fin PCHE, with a 4.83% error in outlet temperature and a 3.33% error in pressure drop. These minor discrepancies are within acceptable limits and can be attributed to several factors, including simplifications in the numerical model such as steady-state assumptions, idealised boundary conditions, and constant material properties. Additionally, the turbulence and heat transfer models used in the simulation may not capture all the intricate flow behaviours within the micro-channels. Experimental uncertainties such as sensor inaccuracies and environmental variations also contribute to the observed differences. Overall, the close match between the results validates the accuracy and reliability of the numerical approach for predicting PCHE performance (Raji et al., 2024).

2. RESULTS AND DISCUSSIONS

3.1. CFD Results of Base Airfoil Fin PCHE

Figures 23 and 24 illustrate the temperature and pressure profiles across the PCHE equipped with the base airfoil fin (NACA0021) arranged in a staggered configuration. The data clearly demonstrate a steady decrease in temperature from 550 K at the inlet to 395.75 K at the outlet. This temperature decline is primarily due to the expanded heat transfer surface area offered by the airfoil fins distributed within the channel, which promote enhanced convection between the hot sCO_2 fluid and the walls (Raji et al., 2024).

Figure 24 depicts the pressure variation across the PCHE equipped with the base airfoil fin arranged in a staggered pattern. The results indicate that there is a modest pressure drop of approximately 14 Pa from the inlet to the outlet of the channel. This pressure loss is primarily caused by the frictional resistance encountered between the sCO_2 fluid and solid surfaces within the channel over its length. The relatively small pressure drop suggests that the design effectively minimises flow resistance while maintaining efficient heat transfer, aligning with the findings reported by Raji et al. (2024).

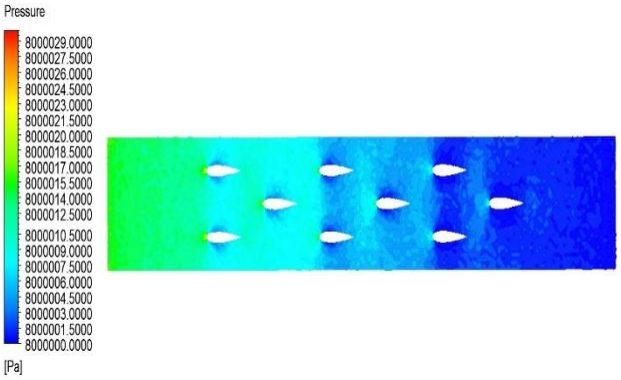

Fig. 24 Pressure distribution over an airfoil fin PCHE

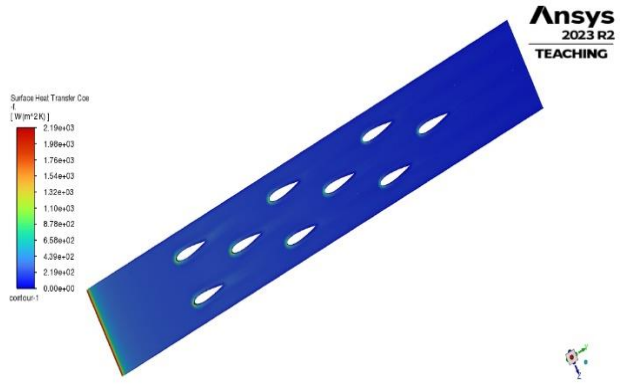

Fig. 25 Heat transfer variation across the base airfoil fin PCHE

Figure 25 represents the heat transfer variation across the base airfoil fin PCHE. It can be clearly seen from the result that the surface heat transfer coefficient for the base airfoil fin model at the exit is 226.37 W/m²K (Raji et al., 2024).

3.2. CFD Results of Different Novel Stepped Airfoil Fin PCHE

Figures 26 to 28 depict the temperature, pressure distribution, and heat transfer characteristics of the stepped airfoil fin PCHE model 9. The temperature contour clearly indicates a substantial drop in fluid temperature from 550 K at the inlet to 350.6 K at the outlet, demonstrating effective thermal energy extraction throughout the flow passage. This pronounced temperature reduction is primarily due to the stepped geometry on the upper surface of the airfoil, which induces localised turbulence and promotes strong flow recirculation zones near the fin surface. These flow disturbances break the thermal boundary layer, enhancing convective mixing between the core and wall regions of the flow. As a result, the local and overall heat transfer coefficient increases significantly, reaching 313.63 W/m²K, which represents a notable improvement over the baseline (non-stepped) airfoil configuration. Figure 29 shows a comparison of velocity and turbulence intensity between the base model and the novel airfoil fin model 9. The results demonstrate that model 9 achieves improved turbulence intensity compared with the base model, which

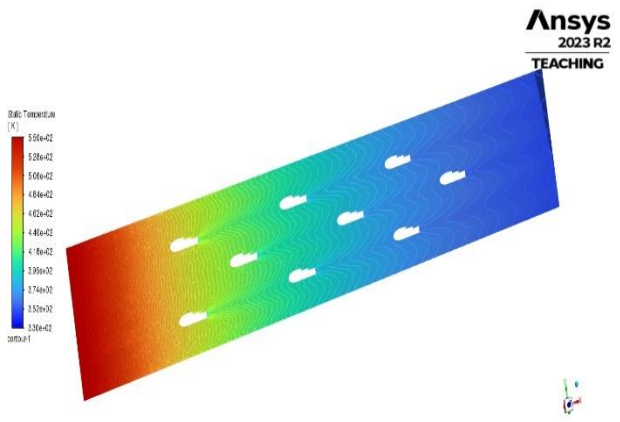

Fig. 26 Temperature variation across the airfoil fin PCHE model 9

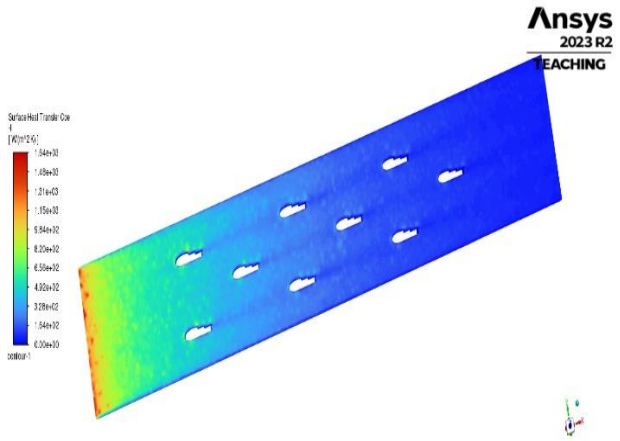

Fig. 27 Heat transfer variation across the airfoil fin PCHE model 9

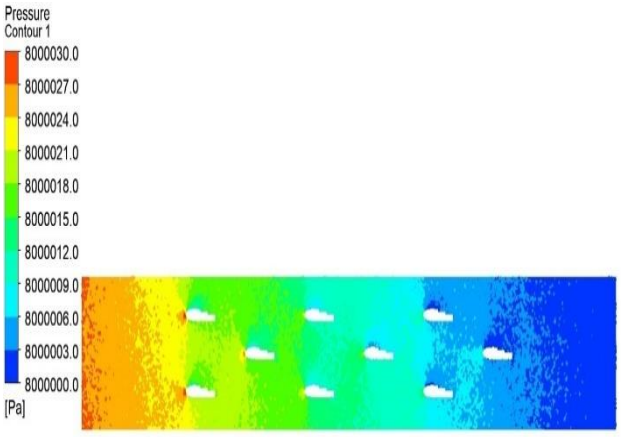

Fig. 28 Pressure distribution over the airfoil fin PCHE model 9

contributes to the enhancement of convective heat transfer. This enhanced thermal performance confirms the effectiveness of the stepped design in promoting heat transfer by intensifying surface interaction and flow disruption.

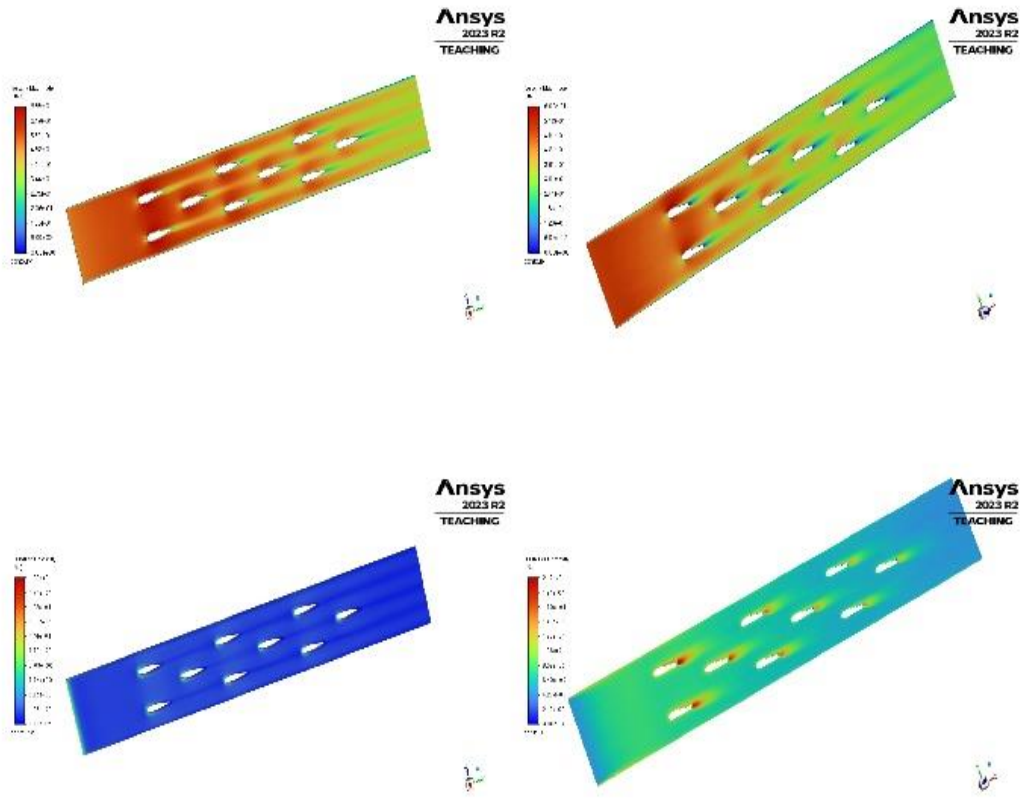

Fig. 29 Velocity and turbulence intensity comparison for base and model 9

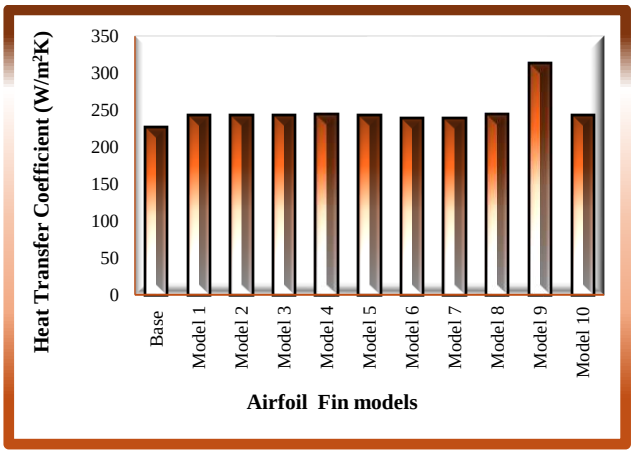

Fig. 30 Heat transfer comparison of various airfoil fin models in PCHE

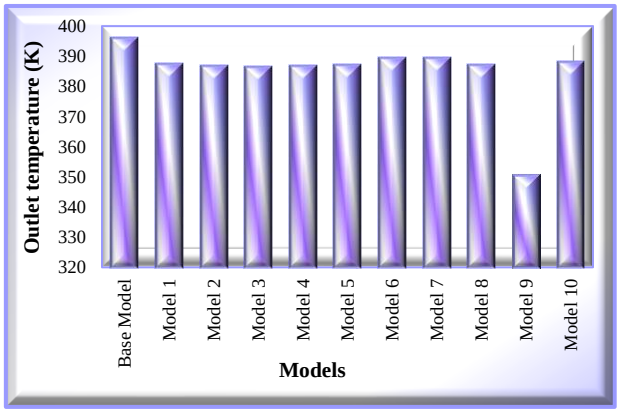

Fig. 31 Comparison of outlet temperature for different airfoil fin models

3.3 Thermohydraulic Performance Comparisons

Figures 30 and 31 present a comparative analysis of the heat transfer coefficients and temperature distributions for various novel stepped airfoil fin models versus the baseline airfoil design. The data clearly demonstrate that all stepped configurations outperform the base model in terms of thermal performance. Among them, airfoil fin model 9 stands out, delivering the highest heat transfer coefficient of 313.63 W/m²K and achieving the lowest outlet temperature of 350.6 K. These results underscore the superior efficiency of model 9 in facilitating thermal energy exchange. The observed enhancement is primarily attributed to the prominent stepped geometry, which promotes strong flow recirculation and increased surface turbulence. These effects disrupt the thermal boundary layer and improve mixing between the cooler wall-adjacent fluid and the hotter core flow, thereby boosting convective heat transfer. The larger and more aggressive step structure in model 9 effectively optimises the interaction between the fluid and the heat exchanger surface, leading to significantly improved thermal performance compared with both the base and other modified models.

Figures 32 and 33 provide a comparative evaluation of the Nusselt number and pressure drop for various novel stepped airfoil fin models relative to the baseline configuration. The results reveal that all modified airfoil

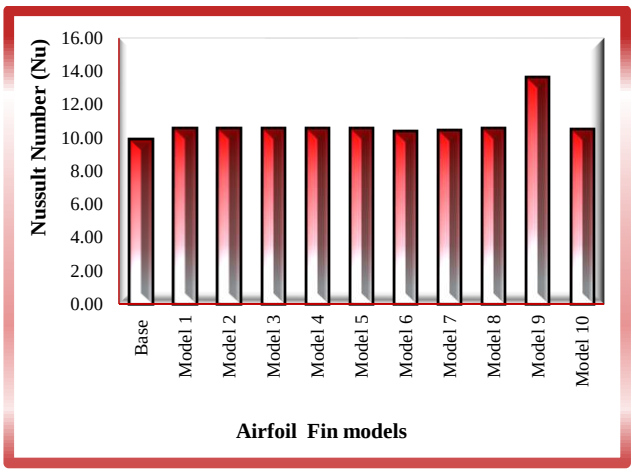

Fig. 32 Variation of Nusselt number for different airfoil Fin models in PCHE

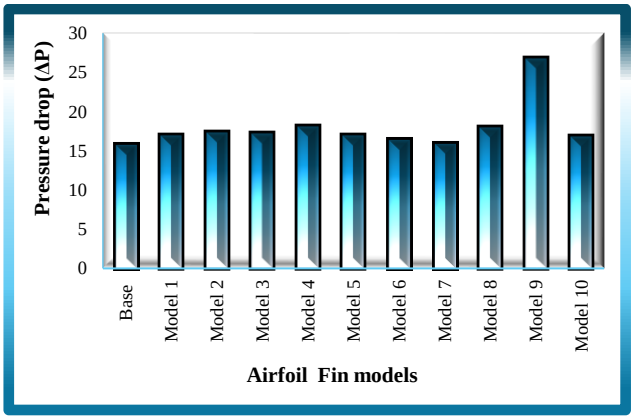

Fig. 33 Variation of pressure drop for different airfoil fin models in PCHE

designs result in a noticeable increase in the Nusselt number, indicating enhanced convective heat transfer performance. However, this improvement is accompanied by a modest rise in pressure drop across the channel. Among the tested models, airfoil fin model 9 achieves the highest Nusselt number of 13.59, along with a pressure drop of 26.9 Pa, demonstrating superior thermohydraulic performance compared with both the base model and other stepped configurations.

The enhanced Nusselt number can be attributed to the stepped geometry, which effectively disrupts the laminar flow near the airfoil surface, introducing localised turbulence and recirculation zones. These disturbances thin the thermal boundary layer, thereby increasing the rate of convective heat transfer. Simultaneously, the abrupt changes in surface contour introduced by the steps generate adverse pressure gradients, particularly near the trailing edge. These gradients lead to flow separation and the formation of low-pressure regions downstream of the steps, contributing to the observed increase in pressure drop. Despite this rise, the pressure loss remains within an acceptable range, making model 9 a promising option for high-performance PCHE applications.

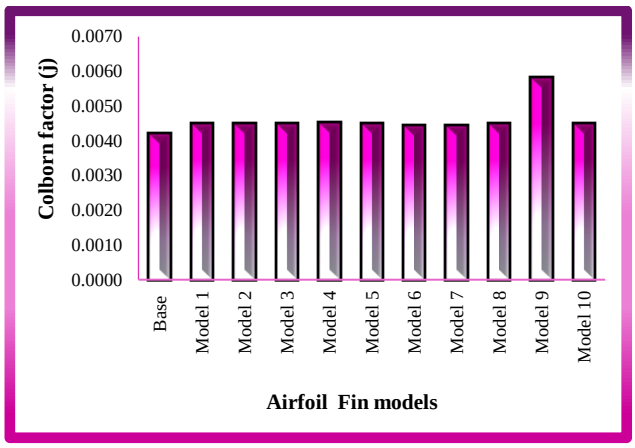

Fig. 34 Variation of Colburn factor for different airfoil fin models in PCHE

Figures 34 and 35 present a comparative analysis of the Colburn factor (j), friction factor (f), and Reynolds number for both the baseline airfoil model and several novel stepped airfoil fin configurations. The Colburn factor (j), which is a dimensionless parameter used to evaluate convective heat transfer performance relative to flow characteristics, is directly proportional to the Nusselt number. As such, higher j-values indicate improved heat transfer efficiency.

The results clearly show that airfoil fin model 9 achieves the highest Colburn factor among all tested configurations, outperforming both the other stepped models and the base airfoil, as illustrated in Fig. 34. This enhancement reflects the model's superior ability to promote convective heat transfer while maintaining a relatively favourable balance with flow resistance. The elevated j-value in model 9 is primarily attributed to its double-stepped geometry, which intensifies turbulence and enhances fluid mixing along the fin surface. These flow modifications improve heat transfer effectiveness without causing an excessive increase in the friction factor, as observed in Fig. 35. Therefore, model 9 demonstrates the best overall thermohydraulic performance, especially under low to moderate Reynolds number conditions.

Conversely, the friction factor is strongly influenced by the pressure drop across the channel. In this context, the PCHE equipped with airfoil fin model 9 exhibits a significantly higher pressure drop, which directly contributes to an increased friction factor when compared with the baseline model and other stepped airfoil fin configurations. This relationship is clearly illustrated in Fig. 35. Additionally, Fig. 36 highlights the differences in Reynolds number observed between the baseline and the stepped airfoil fin models. The Reynolds number, being directly proportional to the hydraulic diameter (D_h) of the channel, varies slightly across all airfoil designs. These variations occur despite maintaining the same mass flow rate or inlet velocity, and they are primarily attributed to the geometric differences that influence the effective hydraulic diameter in each model, as depicted in Fig. 36.

Table 3. Thermohydraulic performance results comparison table for different airfoil models

Airfoil Fin model	Heat Transfer Coefficient h(W/m^{2}K)	Nusselt Number (Nu)	Friction factor (f)	Colburn factor(j)	Reynolds Number (Re)	Pressure drop (ΔP)
Base	226.37	9.87	0.056	0.0042	2555	16
Model 1	242.45	10.54	0.060	0.0045	2547	17.1
Model 2	242.64	10.55	0.061	0.0045	2548	17.5
Model 3	242.45	10.54	0.061	0.0045	2548	17.3
Model 4	243.43	10.58	0.064	0.0045	2547	18.2
Model 5	242.42	10.55	0.060	0.0045	2550	17.1
Model 6	239.03	10.41	0.058	0.0044	2551	16.5
Model 7	238.94	10.41	0.057	0.0044	2554	16.1
Model 8	243.22	10.58	0.064	0.0045	2550	18.1
Model 9	313.63	13.59	0.094	0.0058	2540	26.9
Model 10	242.21	10.50	0.060	0.0045	2541	17

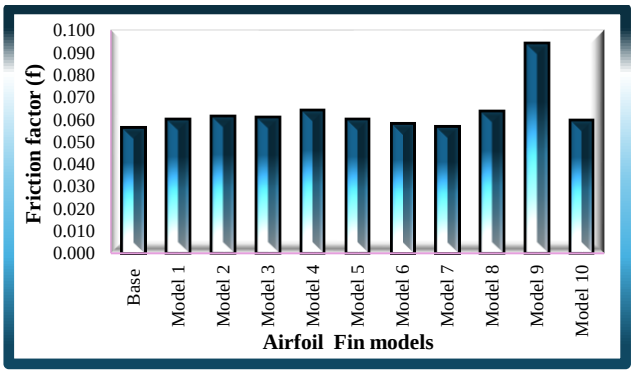

Fig. 35 Variation of friction factor for different airfoil fin models in PCHE

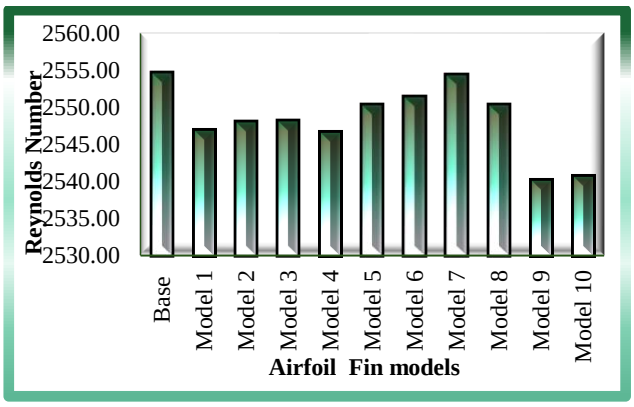

Fig. 36 Variation of Reynolds number for different airfoil fin models in PCHE

The outcomes of the thermohydraulic investigation on PCHE using different novel stepped airfoil fins are shown in Table 3.

3.4. Effect of Reynolds Number on Thermohydraulic Performance of Base and Novel Airfoil Fin Model 9

The thermohydraulic performance of a PCHE is largely governed by its microchannel geometry and the prevailing operating conditions. To gain deeper insight, an extended analysis was carried out to evaluate how

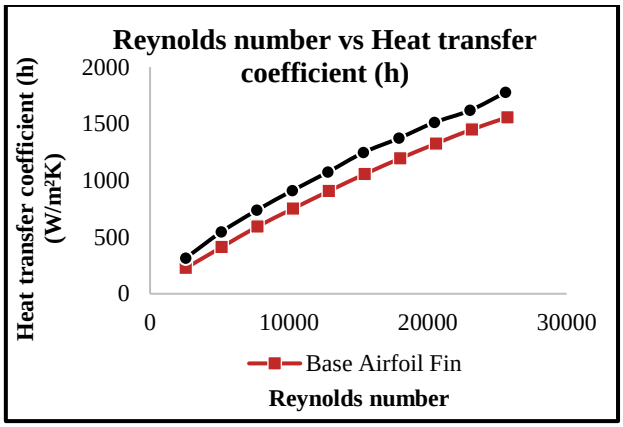

Fig. 37 Heat transfer as a function of Reynolds number

variations in Reynolds number affect the thermal and hydraulic behaviour of both the baseline model and the newly proposed airfoil fin model 9, considered individually. In this study, the Reynolds number was systematically varied within the range of 2,500 to 25,800, corresponding to inlet flow velocities spanning from 0.5 m/s to 5 m/s.

Figures 37 and 38 illustrate the resulting trends in heat transfer coefficient and Nusselt number, respectively, across this range of Reynolds numbers. As the Reynolds number increases, the flow becomes progressively more turbulent, which significantly enhances convective heat transfer. This heightened turbulence intensifies the mixing of fluid layers, thereby leading to a sharp rise in both the heat transfer coefficient and the Nusselt number for both PCHE configurations. The observed trend underscores the strong dependence of thermohydraulic performance on flow regime and channel design.

The novel stepped airfoil fin model 9 demonstrates a marked enhancement in thermal performance compared with the baseline airfoil fin PCHE design. Specifically, the Nusselt number for model 9 shows a substantial increase—approximately 27.37% at lower Reynolds numbers and up to 53.69% at higher Reynolds numbers. This significant improvement can be primarily attributed to the unique stepped geometry of the airfoil surface, which

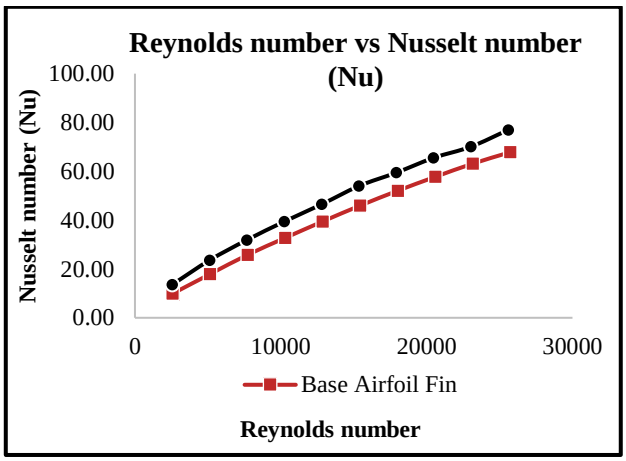

Fig. 38 Nusselt number as a function of Reynolds number

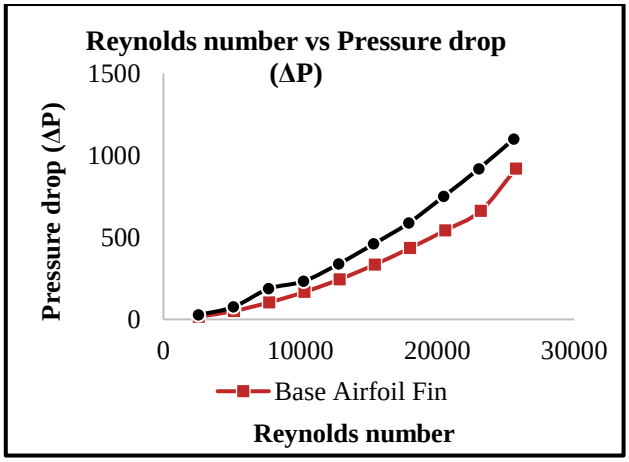

Fig. 39 Pressure drop as a function of Reynolds number

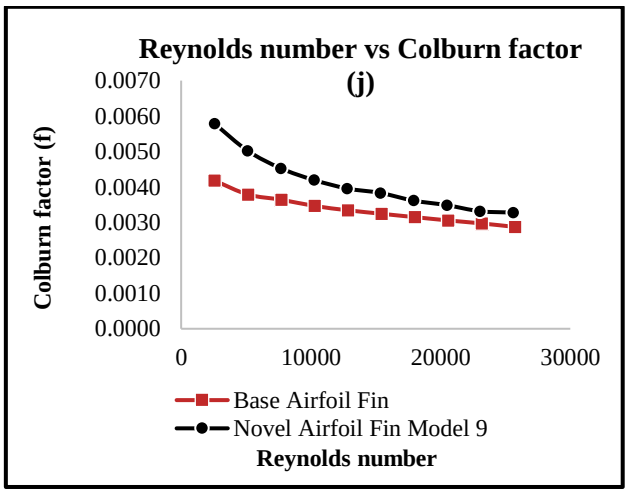

Fig. 40 Colburn factor as a function of Reynolds number

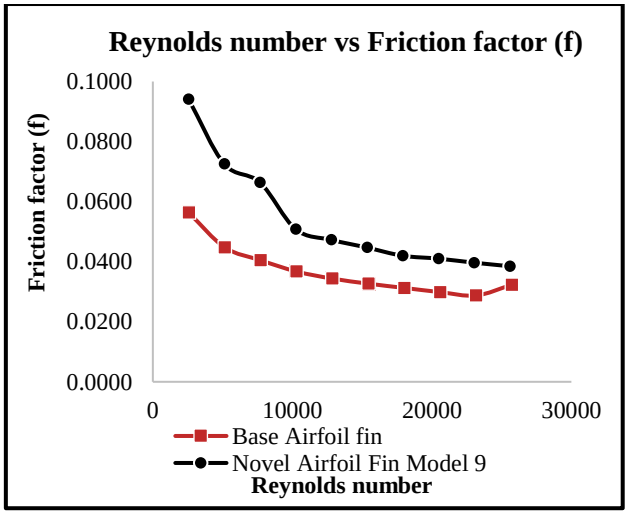

Fig. 41 Friction factor as a function of Reynolds number

effectively disrupts the boundary layer and induces localised turbulence and flow recirculation zones. These flow phenomena enhance convective heat transfer by improving fluid mixing and increasing the contact surface area between the fluid and the channel wall. Consequently, even under high Reynolds number conditions—where laminar-to-turbulent transition and inertial forces dominate—the stepped airfoil fin model 9 maintains superior heat transfer performance over the baseline configuration, making it a highly effective design for improving thermal efficiency in PCHE applications.

Figure 39 presents the relationship between Reynolds number and pressure drop for both the baseline PCHE and the novel stepped airfoil fin model 9. At lower Reynolds numbers, the pressure drops observed in both models are relatively comparable, indicating similar flow resistance under mild flow conditions. However, as the Reynolds number increases, a significant rise in pressure drop is observed, particularly for the novel stepped airfoil fin model 9. This pronounced increase is primarily due to the higher inlet velocities associated with elevated Reynolds numbers, as well as the intensified turbulence and flow disturbances generated by the stepped airfoil surface. The stepped geometry enhances mixing but also introduces additional flow resistance, which contributes to the overall pressure loss.

Figures 40 and 41 further illustrate the variation of the Colburn j-factor (j) and the Fanning friction factor (f) with respect to Reynolds number. The results indicate a clear trend: both the j and f factors decrease with increasing Reynolds number, reflecting their inverse proportionality to Re. Despite this general decline, the novel stepped airfoil fin model 9 consistently exhibits the highest j factor across the entire Reynolds number range, underscoring its enhanced heat transfer capability. Notably, the difference in j factor between the novel stepped model and the baseline airfoil fin diminishes as Reynolds number increases. This suggests that while the stepped design offers a distinct advantage in heat transfer performance at lower Reynolds numbers—where thermal enhancement is more critical—its relative benefit becomes less pronounced under high Reynolds number conditions.

Among the PCHE configurations analysed, the baseline airfoil fin model consistently exhibits the lowest Fanning friction factor (f), indicating superior hydraulic

Table 4 Thermohydraulic performance outcomes of PCHE with base and stepped airfoil fin model 9 for different Reynolds number

Base airfoil fin thermohydraulic performance					
Reynolds Number (Re)	**Nusselt Number (Nu)**	**Friction factor(f)**	**Colburn factor(j)**	**Heat Transfer Coefficient h(W/m²K)**	**Pressure drop (ΔP)**
2574	9.87	0.0563	0.0042	226.37	16
5148	17.89	0.0448	0.0038	410.38	50.9
7722	25.79	0.0405	0.0036	591.56	103.5
10296	32.71	0.0367	0.0035	750.497	167
12870	39.46	0.0344	0.0033	905.2	244.1
15444	45.96	0.0327	0.0032	1054.34	334.3
18018	52.05	0.0313	0.0031	1194.06	435.2
20591	57.73	0.0299	0.0031	1324.32	543.2
23165	63.15	0.0287	0.0030	1448.79	661.4
25739	67.84	0.0323	0.0029	1556.29	918.4
Novel airfoil fin model 9 thermohydraulic performance					
2559	13.59	0.094	0.0058	313.63	26.9
5118	23.58	0.073	0.0050	544.13	75.9
7677	31.88	0.066	0.0045	735.64	186.6
10235	39.41	0.051	0.0042	909.19	232.33
12794	46.46	0.047	0.0040	1071.83	337.7
15353	53.96	0.045	0.0038	1244.89	459.8
17912	59.43	0.042	0.0036	1371.10	587.7
20471	65.49	0.041	0.0035	1510.92	750
23030	70.07	0.040	0.0033	1616.56	918.15
25588	76.93	0.038	0.0033	1774.95	1099.7

efficiency and minimal flow resistance. In contrast, the novel stepped airfoil fin model 9 demonstrates the highest f factor, a result of its enhanced surface complexity and the increased turbulence induced by its stepped geometry. Similar to the trend observed with the Colburn j-factor, the disparity in friction factor between the base and stepped models diminishes as the Reynolds number increases, suggesting that the impact of geometric modifications becomes less pronounced at higher flow rates.

These findings highlight a clear trade-off between thermal and hydraulic performance. The novel stepped airfoil fin model 9 offers the most effective heat transfer across the entire Reynolds number range, outperforming the baseline design due to its ability to promote strong turbulence and improved convective heat exchange. However, this thermal advantage comes at the cost of increased pressure drop and flow resistance. At higher Reynolds numbers, where pressure losses become more critical, the baseline airfoil fin model exhibits better hydraulic performance due to its smoother profile and lower frictional losses. Therefore, the choice between these configurations should consider the specific application requirements—whether prioritising maximum heat transfer or minimising pressure drop.

The outcomes of the thermohydraulic investigation on PCHE using different novel stepped airfoil fins are shown in Table 4.

4. CONCLUSIONS

This study employed computational simulations to investigate the influence of stepped airfoil fin geometries on the thermohydraulic performance of a PCHE. Ten novel stepped airfoil models were analysed and compared against the baseline NACA0021 airfoil.

i) The results demonstrated that all stepped designs improved heat transfer performance, with airfoil fin model 9—characterised by a double-stepped profile and a flattened trailing edge—delivering the most significant enhancement. Specifically, model 9 achieved a 28% increase in heat transfer rate (313.63 W/m²K vs. 226.37 W/m²K) and a 27.37% improvement in the Nusselt number compared with the base model, while maintaining a modest pressure drop increase (less than 26.9 Pa). Additionally, it exhibited a 12.12% to 27.58% higher Colburn j-factor, indicating superior performance in low Reynolds number regimes.

ii) The enhanced performance is primarily attributed to the stepped surface geometry, which induces localised turbulence and disrupts the thermal boundary layer, thereby intensifying convective heat transfer. Although this turbulence slightly increases pressure loss, it remains well within acceptable limits for sCO_2 Brayton cycle systems (below 1 bar).

In conclusion, airfoil fin model 9 proves to be an effective and efficient design for optimising PCHE performance, offering a favourable balance between heat transfer enhancement and pressure drop. It is therefore recommended as a promising candidate for application in sCO_2 Brayton cycle power systems.

COMPETING INTERESTS

The authors affirm that there are no financial or personal relationships that could be viewed as potential

conflicts of interest. Furthermore, this manuscript presents original research that has not been previously published or submitted elsewhere, including in any online or open-access format. The data and findings have been generated with integrity and have not been altered, fabricated, or misrepresented in any form. The authors also confirm that the content is free from plagiarism and that no conflicts of interest exist with respect to the publication of this work.

AUTHORS CONTRIBUTION:

Arul Prakash Raji: Conceptualization, Methodology, Experimental Correlation Studies, Investigation, Resources, Data curation, Writing—original draft preparation; **Sudhakaran Ranganathan:** Methodology, Experimental Correlation Studies, Resources, Data curation, Writing—original draft preparation, Writing—review and editing, Supervision, Project administration; **Beena Stanislaus Arputharaj:** Investigation, Resources, Data curation, and Writing—review and editing; **Vijayanandh Raja:** Methodology, Experimental Correlation Studies, Resources, and Writing—review and editing.

REFERENCES

Ajinkya, M., Ankush, K. J., Sagar, D. K., Jesus, D. O, Clifford, H., Rucha, B., & Pradip, D. (2016). Modeling and analysis of a printed circuit heat exchanger for supercritical CO_2 power cycle applications. *Applied Thermal Engineering*, *109*, Part B., 861-870. https://doi.org/10.1016/j.applthermaleng.2016.05.033

Aneesh, A. M., Atul, S., Atul, S., & Paritosh, C. (2017). Thermo-Hydraulic performance of zigzag, wavy, and serpentine channel based PCHEs. *Fluid Mechanics and Fluid Power – Contemporary Research*, 507–516. https://doi.org/10.1007/978-81-322-2743-4_49

Baik, S., Kim, S. G., Lee, J., & Lee, J. I. (2016). Study on CO_2 – water printed circuit heat exchanger performance operating under various CO_2 phases for SCO_2 power cycle application. *Applied Thermal Engineering*, *113*, 1536–1546. https://doi.org/10.1016/j.applthermaleng.2016.11.132

Dong, E. K., Moo, H. K., Jae, E. C., & Seong, O. K. (2021). Numerical investigation on thermal–hydraulic performance of new printed circuit heat exchanger model. *Nuclear Engineering and Design*, *238*(12), 3269–3276. https://doi.org/10.1016/j.nucengdes.2008.08.002

Fei, C., Lishen, Z., Xiulan, H., Jufeng, Li., Hang, Z., & Zhigang, L. (2017). Comprehensive performance comparison of airfoil fin PCHEs with NACA series airfoil. *Nuclear Engineering and Design*, *315*, 42-50. https://doi.org/10.1016/j.nucengdes.2017.02.014

Chhaparwal, G. K., Rahul, Goyal., Ankur, S., Ashish, G., Ankit, D. O., Md Irfanul, H. S., Natrayan, L., Laveet, K., & Sonawane, C. (2024). Numerical and experimental investigation of a solar air heater duct with circular detached ribs to improve its efficiency. Case Studies in Thermal Engineering, 60, 104780. https://doi.org/10.1016/j.csite.2024.104780

Ganeshkumar, S., Kumar, A., Maniraj, V., Suresh Babu, Y., Alok Kumar, A., Ashish Goyal., Iman Kareem K., Kuldeep, K. S., Prakash, C., Altuijri, R., Ijaz Khan, M., & Ahmed M, H. (2024). Investigations on cooling heat transfer of CO_2-based mixtures in a novel airfoil fin mini-channel at supercritical pressure. *Arabian Journal of Chemistry*, *16(10)*, *105173.* https://doi.org/10.1016/j.arabjc.2023.105173

Gopinath, V., Krishna Priya, M., Rajeshwaran, V., Sudhagaran, D., Shyam Sundar, J., Arul Prakash, R., Beena Stanislaus, A., Parvathy, R., Senthil Kumar, M., & Vijayanandh, R. (2024). Design and Multi-Perspective Investigations on the Aerodynamic Performance Factors of Conventional and Advanced UAV's Micro Gas-Turbine Engine Nozzles Through Validated CFD Approach. *International Journal of Fluid Mechanics Research*, *51*(2), 15–64. https://doi.org/10.1615/InterJFluidMechRes.2024051464

Haiyan, Z., Jiangfeng, Guo., Xinying, C., Jingzhi, Z., Xiulan, H., Huzhong, Z., Keyong, C., & Zengxiao H. (2021). Experimental and numerical investigations of thermal-hydraulic characteristics in a novel airfoil fin heat exchanger. *International Journal of Heat and Mass Transfer*, *175*, https://doi.org/10.1016/j.ijheatmasstransfer.2021.121333

Haiyan, Z., Junfeng, W., Jun, P., Zicheng, H., & Ziyi, S. (2024). Exploring the potential of nano technology: A assessment of nano-scale multi-layered-composite coatings for cutting tool performance. *Applied Thermal Engineering*, *255*, *124010.* https://doi.org/10.1016/j.applthermaleng.2024.124010

In, H. K., & Hee, C. N. (2013). Thermal–hydraulic physical models for a Printed Circuit Heat Exchanger covering He, He–CO_2 mixture, and water fluids using experimental data and CFD. *Experimental Thermal and Fluid Science*,*48*, 213-221. https://doi.org/10.1016/j.expthermflusci.2013.03.003

Ishizuka, T., Kato, Y., Muto, Y., Konstantin, N., & Tri Lam, N. (2006). *Thermal-hydraulic characteristics of a printed circuit heat exchanger in a Supercritical CO_2 loop.* The 11th International Topical Meetingon Nuclear Reactor Thermal-Hydraulics, NURETH 11th-218. https://doi.org/10.1016/j.ijrefrig.2005.11.005

Jin, G. K., Tae, H. K., Hyun, S. P., Jae, E. C., & Moo, H. K. (2016). Optimization of airfoil-type PCHE for the recuperator of small-scale Brayton cycle by cost-based objective function. *Nuclear Engineering Design*, *298*, 192–200. https://doi.org/10.1016/j.nucengdes.2015.12.012

Joo Hyun, P., & Moo Hwan, K. (2024). Experimental investigation on comprehensive thermal-hydraulic performance of supercritical CO_2 in a NACA 0020 airfoil fin printed circuit heat exchanger. *International Journal of Heat and Mass Transfer, 220, 124947*. https://doi.org/10.1016/j.ijheatmasstransfer.2023.124947

Karthigairajan, M., Seeniappan, K., Balaji, N., Natrayan, L. Salman, B. S., & Ravi, D. (2025). *Performance analysis of graphene-coated heat pipe heat exchangers for automobile exhaust cooling and purification*. SAE Technical Paper 2025-01-5006. https://doi.org/10.4271/2025-01-5006.

Kodi, R., Ravuri, M., Gulle, N., Ganteda, C., Khan, S. U., & Ijaz Khan, M. (2022). Hall and ion slip radiative flow of chemically reactive second grade through porous saturated space via perturbation approach. *Waves in Random and Complex Media*, 1–17. https://doi.org/10.1080/17455030.2022.2108555

Kumar, R., Ravi Kumar, D., Ranjeet Kumar, A., Pankaj S., Anil Singh, Y., Kuldeep K. S., Ijaz Khan, M., & Sana Ben, M. (2023). Current development of carbide free bainitic and retained austenite on wear resistance in high silicon steel. *Journal of Materials Research and Technology*, *24*, 9171-9202. https://doi.org/10.1016/j.jmrt.2023.05.067

Kun, X., Xiang, Z., Zhihui, X., Fankai, M., Zhuoqun, L., & Xiangkun, J. (2023). Thermal-hydraulic characteristics of carbon dioxide in printed circuit heat exchangers with staggered airfoil fins. *Processes, 11(8), 2244*. https://doi.org/10.3390/pr11082244

Lei, L., Ting, M., Xiang, Y, X., Min, Z, & Qiuwang, W. (2014a). Optimization of fin arrangement and channel configuration in an Airfoil Fin PCHE for supercritical CO_2 cycle. *Applied Thermal Engineering*, *70*(1), 867-875. https://doi.org/10.1016/j.applthermaleng.2014.05.040

Lei, L., Ting, M., Xiang, Y, X., Min, Z, & Qiuwang, W. (2014b). Study on heat transfer and pressure drop performances of airfoil-shaped printed circuit heat exchanger. *Chemical Engineering Transactions*, *39*, 895-900. https://doi.org/10.3303/CET1439150

Lei, X., Zhang, Q., Zhang, J., & Li, H. (2017). Experimental and numerical investigation of convective heat transfer of supercritical carbon dioxide at low mass fluxes. *Applied Sciences*, *7*(12), 1260. https://doi.org/10.3390/app7121260

Minghui, C., Xiaodong, S., Richard, N. C., Isaac, S., Vivek, U., & Piyush, S. (2016). Pressuredrop and heat transfer characteristics of a high-temperature printed circuit heat exchanger. *Applied Thermal Engineering, 108*, 1409–1417, https://doi.org/10.1016/j.applthermaleng.2016.07.149

Sandeep, R. P., Mark, A., & Devesh, R. (2018, March 27-29). *Thermal-hydraulic performance of discontinuous fin heat exchanger geometries using Supercritical CO_2 as the working fluid*. The 6th International Supercritical CO_2 Power Cycles Symposium, Pittsburgh, Pennsylvania. https://sco2symposium.com/papers2018/heatexchangers/130_Paper.pdf.

Pinaa, P., Ferrãoa, J., & Fournierb, C. (2019). *Study of the printed circuit heat exchanger for supercritical CO_2 application.* 2nd International Conference on Sustainable Energy and Resource Use in Food Chains, ICSEF2018.DOI: https://doi.org/10.1016/j.egypro.2019.02.066

Raghunath, K., Ramachandra Reddy, V., Ijaz Khan, M., Sherzod Shukhratovich, A., Habibullah., Boudjemline, A., H., Mohamed Boujelbene., & Yassine, B. (2023). Unsteady magneto-hydro-dynamics flow of Jeffrey fluid through porous media with thermal radiation, Hall current and Soret effects. *Journal of Magnetism and Magnetic Materials, 582*, 171033. https://doi.org/10.1016/j.jmmm.2023.171033

Raji, A. P., Ranganathan, S., Stanislaus Arputharaj, B., & Vijayanandh, R. (2024). Thermostructural analysis on airfoil fin printed circuit heat exchanger using supercritical CO_2. *Journal of Thermal Analysis and Calorimetry*, *149*(9), 4153–4177. https://doi.org/10.1007/s10973-024-12925-y.

Saeed, M., & Kim, M. (2017). Thermal and hydraulic performance of sCO_2 PCHE with different fin Configurations. *Applied Thermal Engineering*, *127*, 975-985. https://doi.org/10.1016/j.applthermaleng.2017.08.113

Sandeep, R. P., Eric, U., Jacob, A. Mc, F., Devesh, R., & Mark, H. A. (2014). Effect of buoyancy on heat transfer characteristics of supercritical carbon dioxide in the heating mode. AIAA AVIATION Forum, Atlanta, GA,11th AIAA/ASME Joint Thermophysics and Heat Transfer Conference,16-20. https://doi.org/10.2514/6.2014-3359

Seo, J. W., Kim, Y. H., Kim, D., Choi, Y. D., & Lee, K. J. (2015). Heat transfer and pressure drop characteristics in straight microchannel of printed circuit heat exchangers. *Entropy*, *17*(5), 3438-3457. https://doi.org/10.3390/e17053438

Seong, G. K., Youho, L., Yoonhan, A., & Jeong, I. (2016). CFD aided approach to design printed circuit heat exchangers for supercritical CO_2 Brayton cycle application. *Annals of Nuclear Energy, 92*, 175–185. https://doi.org/10.1016/j.anucene.2016.01.019

Sheikholeslami, M., & Abd Ali, F. A. M. (2024a). Influence of vortex generator on performance of concentrated solar photovoltaic module in existence of heat sink. *Applied Thermal Engineering*, *253*, 123758. https://doi.org/10.1016/j.applthermaleng.2024.123758

Sheikholeslami, M., & Khalili, Z. (2024b). Simulation for impact of nanofluid spectral splitter on efficiency of concentrated solar photovoltaic thermal system. *Sustainable Cities and Society, 101, 10513.* https://doi.org/10.1016/j.scs.2023.105139

Sheikholeslami, M., Khalili, Z., Scardi, P., & Ataollahi, N. (2024c). Environmental and energy assessment of photovoltaic-thermal system combined with a reflector supported by nanofluid filter and a sustainable thermoelectric generator. *Journal of Cleaner Production, 438*, 140659. https://doi.org/10.1016/j.jclepro.2024.140659

Su-Jong, Y., Piyush, S., & Eung-Soo, K. (2014). Numerical study on crossflow printed circuit heat exchanger for advanced small modular reactors. *International Journal of Heat and Mass Transfer, 70*, 250-263. https://doi.org/10.1016/j.ijheatmasstransfer.2013.10.079

Tae, H. K., Jin, G. K., Sung, H. Y., Hyun, S. P., Moo, H. K., Jae, & Cha, E. (2015). Numerical analysis of air-foil shaped fin performance in printed circuit heat exchanger in a supercritical carbon dioxide power cycle. *Nuclear Engineering and Design, 288*, 110–118. https://doi.org/10.1016/j.nucengdes.2015.03.013

Thangaraj, J., Senthil Kumar, M., Parvathy, R., Safiah, Z., Rajkumar, R., Hussein, A. Z. AL-bonsrulah., Beena Stanislaus, A., Hari Prasath, J., & Vijayanandh, R. (2023). Design, multi-perspective computational investigations, and experimental correlational studies on conventional and advanced design profile modified hybrid wells turbines patched with piezoelectric vibrational energy harvester devices for coastal regions. *Processes, 11*(9), 2625. https://doi.org/10.3390/pr11092625

Usman, M., Ijaz Khan, M., Shah, F., Khan, SU., Ghaffari, A., & Chu, Y. M. (2022). Heat and mass transfer analysis for bioconvective flow of Eyring Powell nanofluid over a Riga surface with nonlinear thermal features. *Numerical Methods for Partial Differential Equations. 38*, 777–793. https://doi.org/10.1002/num.22696

Veeraperumal Senthil Nathan, J., Pisharam, A., Sourirajan, L., Baskar, S., Gopinath, V., Beena Stanislaus, A., Natrayan, L., Pradesh, S., & Vijayanandh, R. (2025). *Operation of advanced flying wing UAV: Examination of structural performance under aberrant pressure and thermal loading conditions with integrated computational study*. SAE Technical Paper 2025-28-0060. https://doi.org/10.4271/2025-28-0060.

Wen-xiao, C., Xiong-hui, L., Ting, M., Yi-tung, C., & Qiu-wang, W. (2017). Experimental investigation on sCO_2-water heat transfer characteristics in a printed circuit heat exchanger with straight channels. *International Journal of Heat and Mass Transfer. 113*, 184–194, https://doi.org/10.1016/j.ijheatmasstransfer.2017.05.059

Wen-xiao, C., Xiong-hui, L., Ting, M., Yi-tung, C., & Qiu-wang, W. (2016). Study on hydraulic and thermal performance of printed circuit heat transfer surface with distributed airfoil fins. *Applied Thermal Engineering, 114*, 1309–1318. https://doi.org/10.1016/j.applthermaleng.2016.11.187

Xinying, C., Jiangfeng, G., Xiulan, H., Keyong, C., Haiyang, & Mengru, X. (2018). Numerical study on novel airfoil fins for printed circuit heat exchanger using supercritical CO_2. *International Journal of Heat and Mass Transfer, 121*, 354-366. https://doi.org/10.1016/j.ijheatmasstransfer.2018.01.015

Xu, X. Y., Wang, Q. W., Li, L., Ekkad, S. V., & Ma, T. (2015). Thermal-hydraulic performance of different discontinuous fins used in a printed circuit heat exchanger for supercritical CO_2. *Numerical Heat Transfer, Part A: Application, 68*, 1067-1086, https://doi.org/10.1080/10407782.2015.1032028

Yu-Ming, C., Khan, Ijaz Khan, M., Hassan, W., Umar, F., Sami Ullah, K., & Mubbashar, N. (2021). Numerical simulation of squeezing flow Jeffrey nanofluid confined by two parallel disks with the help of chemical reaction: effects of activation energy and microorganism. *International Journal of Chemical Reactor Engineering, 19*(7), 2021, 717-725. https://doi.org/10.1515/ijcre-2020-0165

Yun-Jie, X., Faisal, S., Ijaz Khan, M., Naveen Kumar, R., Punith Gowda, R. J., Prasannakumara, B. C., Malik, M. Y., & Sami Ullah, K. (2022). New modeling and analytical solution of fourth grade (non-Newtonian) fluid by a stretchable magnetized Riga device. *International Journal of Modern Physics C, 33*(1), 2250013. https://doi.org/10.1142/S0129183122500139

Zhao, Z., Zhao, K., Jia, D., Jiang, P., & Shen, R. (2017). Numerical investigation on the flow and heat transfer characteristics of supercritical liquefied natural gas in an airfoil fin printed circuit heat exchanger. *Energies, 10*(11), 1828. https://doi.org/10.3390/en10111828

Zhongchao, Z., Xudong, C., Xiao, Z., Xiaolon M., & Shan, Y. (2020). Experimental and numerical study on thermal-hydraulic performance of printed circuit heat exchanger for liquefied gas vaporization. *Energy Science & Engineering, 8*(2), 426–440. https://doi.org/10.1002/ese3.525